Dynactin-dependent cortical dynein and spherical spindle shape correlate temporally with meiotic spindle rotation in *Caenorhabditis elegans*

Marina E. Crowder, Jonathan R. Flynn, Karen P. McNally, Daniel B. Cortes, Kari L. Price, Paul A. Kuehnert, Michelle T. Panzica, Armann Andaya, Julie A. Leary, and Francis J. McNally
Department of Molecular and Cellular Biology, University of California, Davis, Davis, CA 95616

ABSTRACT **Oocyte meiotic spindles orient with one pole juxtaposed to the cortex to facilitate extrusion of chromosomes into polar bodies. In *Caenorhabditis elegans*, these acentriolar spindles initially orient parallel to the cortex and then rotate to the perpendicular orientation. To understand the mechanism of spindle rotation, we characterized events that correlated temporally with rotation, including shortening of the spindle in the pole-to pole axis, which resulted in a nearly spherical spindle at rotation. By analyzing large spindles of polyploid *C. elegans* and a related nematode species, we found that spindle rotation initiated at a defined spherical shape rather than at a defined spindle length. In addition, dynein accumulated on the cortex just before rotation, and microtubules grew from the spindle with plus ends outward during rotation. Dynactin depletion prevented accumulation of dynein on the cortex and prevented spindle rotation independently of effects on spindle shape. These results support a cortical pulling model in which spindle shape might facilitate rotation because a sphere can rotate without deforming the adjacent elastic cytoplasm. We also present evidence that activation of spindle rotation is promoted by dephosphorylation of the basic domain of p150 dynactin.**

Monitoring Editor
Fred Chang
Columbia University

Received: May 19, 2015
Revised: Jun 17, 2015
Accepted: Jun 24, 2015

INTRODUCTION

Female meiotic spindles are positioned asymmetrically within oocytes, with one spindle pole juxtaposed closely against the cortex. This perpendicular spindle positioning facilitates expulsion of half of the homologous chromosomes into a small polar body during anaphase I and expulsion of half of the remaining sister chromatids into a second polar body during anaphase II. In *Caenorhabditis elegans*, a stereotypical series of microtubule-dependent events orients the female meiotic spindle in a perpendicular orientation at the cortex. The first of these events occur before ovulation, when the germinal vesicle moves toward the future anterior cortex in a kinesin-1–dependent manner (McCarter *et al.*, 1999; McNally *et al.*, 2010). During and after ovulation, the meiosis I spindle assembles several micrometers from the cortex, moves close to the cortex, and adopts a roughly parallel orientation, with each pole nearly equidistant from the cortex (Yang *et al.*, 2003). Early translocation of the germinal vesicle to the cortex is independent of the anaphase-promoting complex (APC) but dependent on kinesin-1 and its binding partner KCA-1 (Yang *et al.*, 2005; McNally *et al.*, 2010). In kinesin-1– or KCA-1–depleted embryos, spindles assemble far from the cortex and remain there during metaphase.

Metaphase I spindles maintain a constant length and parallel orientation at the cortex for an average of 7 min after ovulation. Then a coordinated series of APC-dependent events initiates, which results in positioning of the spindle perpendicular to the cortex and extrusion of chromosomes into a polar body. First, the spindle shortens along the pole–pole axis while maintaining a parallel orientation relative to the cortex. One spindle pole then moves toward the cortex in a process referred to as spindle rotation. Anaphase chromosome separation initiates after rotation when the spindle is at its shortest length. The spindle then elongates in an anaphase B–like process (Yang *et al.*, 2003, 2005) concurrent with formation and ingression of the polar body contractile ring (Dorn *et al.*, 2010;

This article was published online ahead of print in MBoC in Press (http://www.molbiolcell.org/cgi/doi/10.1091/mbc.E15-05-0290) on July 1, 2015.

Address correspondence to: Francis J. McNally (fjmcnally@ucdavis.edu).

Abbreviations used: aa, amino acid; APC, anaphase-promoting complex; DAPI, 4′,6-diamidino-2-phenylindole; DMSO, dimethyl sulfoxide; GFP, green fluorescent protein; PA, purvalanol A; RNAi, RNA interference.

Fabritius *et al.*, 2011). This cycle repeats during meiosis II (Yang *et al.*, 2003).

Spindle rotation is blocked in mutants or RNA interference (RNAi) depletions of katanin (McNally *et al.*, 2006), dynein heavy chain (Ellefson and McNally, 2009; van der Voet *et al.*, 2009) or ASPM-1 (van der Voet *et al.*, 2009). In each of these genotypes, spindle shortening still occurs, but spindles are longer in the pole–pole axis at metaphase (McNally *et al.*, 2006; Ellefson and McNally, 2011; Connolly *et al.*, 2014) and thus do not reach the length at which wild-type spindles rotate. Thus it remains possible that spindles must shorten to a particular length before rotation can occur.

In kinesin-1– or KCA-1–depleted embryos, a pole-first late translocation of the spindle to the cortex occurs during the spindle-shortening cycle. Late translocation in a kinesin mutant and wild-type spindle rotation both require the APC and cytoplasmic dynein (Yang *et al.*, 2005; Ellefson and McNally, 2009), suggesting that both spindle movements occur by the same mechanism but from different starting positions. Dynein heavy chain accumulates on meiotic spindle poles in an APC-dependent manner just before initiation of late translocation or wild-type spindle rotation (Ellefson and McNally, 2009), further supporting a direct mechanistic link between spindle rotation and cytoplasmic dynein. Inhibition of cyclin B/CDK-1 with purvalanol A (PA) in metaphase I–arrested, APC-depleted embryos was sufficient to induce spindle shortening, accumulation of dynein on spindle poles, accumulation of dynein on the cortex, and dynein-dependent spindle rotation (Ellefson and McNally, 2011). This result indicated that the APC induces these events through proteolysis of cyclin B and subsequent dephosphorylation of cyclin B/CDK-1 substrates.

A likely target of cyclin B/CDK1 phosphorylation is the p150 dynactin subunit, DNC-1. The basic, serine-rich domain of DNC-1 had the highest density of phosphorylation sites of any dynein regulator in a *C. elegans* phosphoproteome study (Bodenmiller *et al.*, 2008; Zielinska *et al.*, 2009). This suggested the hypothesis that phosphorylation of the basic domain might inhibit microtubule binding by the adjacent CAP-Gly domain during metaphase. APC-dependent dephosphorylation of this region of DNC-1 would then induce microtubule binding by the adjacent CAP-Gly domain. Because the CAP-Gly domain is required for dynein-dependent movement against a high load in vivo (Moore *et al.*, 2009), binding of the CAP-Gly domain to microtubules might drive spindle rotation. This model is supported by the finding that inhibition of cyclin B/CDK-1 activity could induce spindle association of a *C. elegans* DNC-1 CAP-Gly + basic domain:green fluorescent protein (GFP) fusion in MG132-arrested *Xenopus* A6 cells (Ellefson and McNally, 2011).

The most commonly investigated examples of spindle positioning have been explained with a cortical pulling model. In a cortical pulling model, a microtubule motor protein, most often cytoplasmic dynein, is anchored to the cell cortex and interacts with the plus ends of astral microtubules. The minus ends of these microtubules are anchored in either a centriole-containing centrosome, as in animal cells, or in a spindle pole body, as in fungi. The minus end–directed motor activity of dynein then generates a transient pulling force on the centrosome or spindle pole body that constitutes one spindle pole (Kotak and Gonczy, 2013; Lu and Johnston, 2013; McNally, 2013). A cortical pulling model is consistent with the inward deflection of the cortex observed upon micromanipulation of the meiotic spindles of *Chaetopterus* oocytes (Lutz *et al.*, 1988). However, the female meiotic spindles of many species, including *C. elegans*, do not have centriole-containing centrosomes at their poles nor obvious astral microtubules emanating from the poles (Albertson and Thomson, 1993). Thus it has been unclear whether a cortical pulling mechanism can explain the positioning of acentriolar female meiotic spindles.

In this article, we address several unresolved questions regarding meiotic spindle rotation. What is the relationship between spindle shortening and spindle rotation? Are cortical dynein and astral microtubules, which would support a cortical pulling model, present during rotation? What is the mechanism by which CDK-1 inactivation induces dynactin association with meiotic spindles?

RESULTS

Spindles rotate when they are nearly spherical, at a precise aspect ratio, not length

We previously reported that *C. elegans* meiotic spindles initiate rotation to place one spindle pole at the cortex when they have shortened to a defined pole-to-pole length. However, the rotation length also corresponds to a defined spherical shape during both meiosis I and meiosis II (Table 3 in Yang *et al.*, 2003; Figure 1, A–D). At metaphase, the MI spindle is an 8-µm-long, 6-µm-wide prolate ellipsoid, whereas at rotation, the spindle is a sphere with a diameter of 4.8 µm (Yang *et al.*, 2003). The combined reduction in volume and change in shape might be advantageous because it would reduce the rotational frictional drag coefficient from 900 to 350 pN s µm. However, the force needed to overcome this frictional drag during a 90° rotation would only change from 3.5 to 1.5 pN (see the Supplemental Materials). These values are small relative to the 1–6 pN generated by a single dynein motor (Nicholas *et al.*, 2015), and the majority of the drag reduction is due to the reduced volume rather than the change in shape (see the Supplemental Materials). Another explanation as to why it might be advantageous for the rotating spindle to be spherical is that an ellipsoid rotating about its minor axis displaces adjacent elastic cytoplasm. The Young's modulus, G^*, describes an elastic material's resistance to deformation. Using the Young's modulus of 15 µM F-actin (1 pN/µm^2) or that of a solution of F-actin cross-linked by α-actinin (30 pN/µm^2) at 0.01 Hz (Wachsstock *et al.*, 1993) as an approximation for the cytoplasm and half the cross-sectional area of an ellipsoid metaphase I spindle (18.5 µm^2), the elastic resistance to the rotating metaphase spindle could be from 18.5 to 555 pN. In contrast, a sphere can rotate on its own axis without displacing adjacent cytoplasm and thus experiences elastic resistance of 0. To test whether rotation initiation correlates more closely with spindle length or spindle shape, we analyzed three situations in which meiotic spindles might have altered length/width scaling: triploid *C. elegans*, tetraploid *C. elegans*, and *Pellioditis typica*, a nematode species with a genome size three times that of *C. elegans* (Flemming *et al.*, 2000). We were limited to fixed immunofluorescence for the analysis of tetraploids and *P. typica*. Therefore we first needed to devise a way to define a fully rotated spindle so that we could measure the size and geometry of unrotated and rotated spindles.

We previously used a "rotation index" to quantify rotation of a spindle, calculated as the ratio of the distances of each spindle pole to the closest point on the cortex (Ellefson and McNally, 2011). Using a plasma membrane marker (GFP:pleckstrin homology domain) and improved time-lapse imaging, we discovered that a significant space (>1 µm) can be seen between the spindle poles and plasma membrane before rotation (Figure 1A). After rotation, one pole is tightly juxtaposed against the plasma membrane. This additional distinction is significant because spindles sometimes appear to be partially rotated before initiating movement of one pole to the cortex (Figure 1B and Supplemental Figure S1). Therefore we used

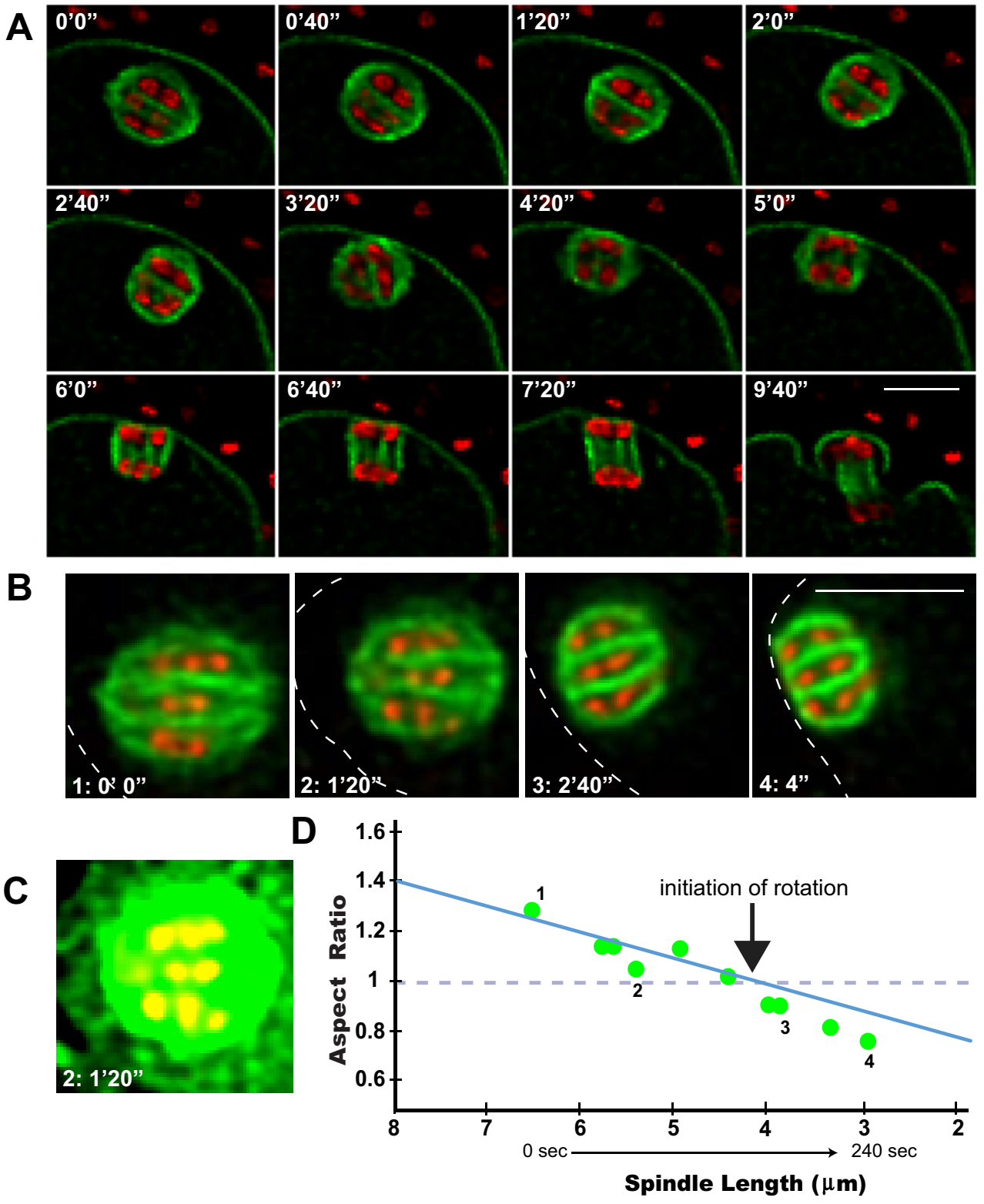

FIGURE 1: *C. elegans* meiotic spindles shorten and change aspect ratio before initiating spindle rotation. (A) Time-lapse sequence of meiosis I spindle rotation in an embryo expressing GFP:tubulin, GFP:PH, and mCherry:histone H2B. A 90° rotation initiates between 2'40'' and 3'20''. (B) Time-lapse sequence of a 45° rotation in an embryo expressing GFP:tubulin and mCherry:histone. The edge of the cortex drawn in B was based on contrast-enhanced images as in C. (D) Spindle aspect ratio plotted against spindle length for the time-lapse sequence in B. The best-fit line determined by linear regression is shown. All points below the dotted horizontal line represent spindles that have initiated or completed a concerted movement of one pole to the cortex. Bars, 5 μm.

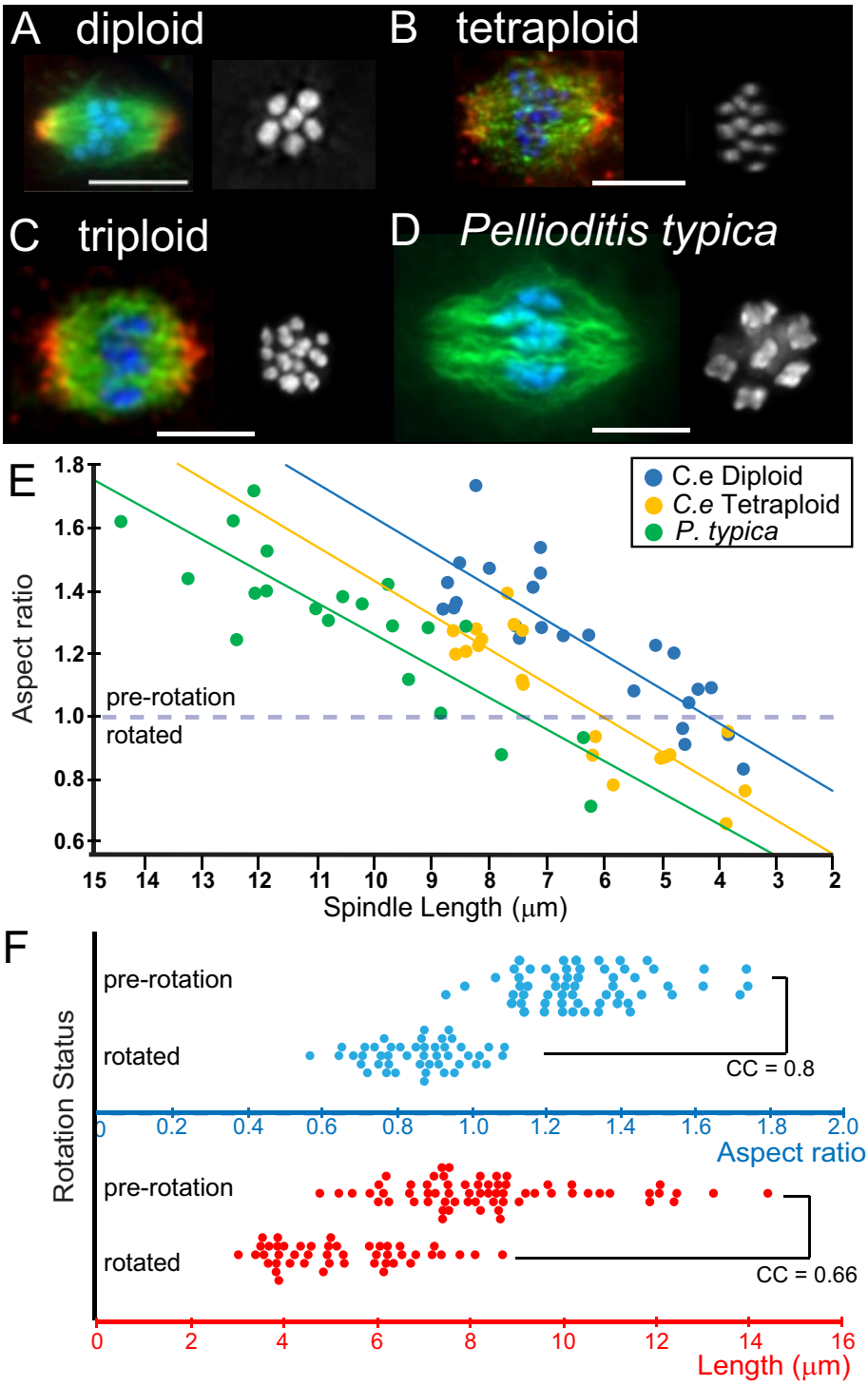

FIGURE 2: Spindle aspect ratio correlates with rotation. (A–D) Representative maximum intensity projections of *z*-stacks of metaphase I spindles fixed and stained with anti-tubulin (green) and anti-ASPM-1 (red) antibodies and DAPI (blue). Grayscale images show DAPI staining of chromosomes viewed down the pole–pole axis. Triploid *C. elegans* were the F1 progeny of diploid males crossed with tetraploid hermaphrodites. (E) The aspect ratio and length were determined from 3D reconstructions and *z*-projections of each image, and the best-fit line was determined by linear regression. Spindles below the dotted horizontal line were rotated, and those above the line were not rotated. Points on the line indicate spindles with an intermediate orientation. (F) Binary rotation status (prerotation vs. rotated) was plotted on the *y*-axis against spindle aspect ratio (length/width; blue symbols) or against spindle length (red symbols) on the *x*-axis. The 112 data points include spindles from diploid, triploid, and tetraploid *C. elegans*, as well as *P. typica*. CC, correlation coefficient. Bars, 5 μm.

lack of a visible space between the cortex and closest spindle pole as an additional criterion for scoring a rotated spindle. Rotation status, spindle length, and spindle width were determined from single–focal plane time-lapse images or three-dimensional (3D) reconstructions (see *Materials and Methods*) of fixed embryos stained with anti-tubulin, anti-ASPM-1, and 4′,6-diamidino-2-phenylindole (DAPI). The aspect ratio (spindle length divided by spindle width) was plotted on the *y*-axis, and spindle length was plotted on the *x*-axis. For wild-type, diploid *C. elegans*, the observed data points from time-lapse sequences (Figure 1D) fell within a 10% error margin of the calculated line of best fit from fixed images (Figure 2E; slope, 0.1). In time-lapse sequences of living diploid *C. elegans*, initiation of rotation occurred at an aspect ratio of ≤1.0 (Figure 1D). In fixed diploid *C. elegans* embryos, spindles with aspect ratios >1.0 were always unrotated, whereas spindles with aspect ratios <1.0 were most often fully rotated; however, a few spindles had a rotation index and cortical spacing that suggested a transitory stage (Figure 2E). These correlations justify the use of 3D reconstructions of fixed embryos to address the relationship between spindle length, aspect ratio, and rotation initiation.

Diploid *C. elegans* have six bivalents at metaphase I (Figure 2A), tetraploids have 12 bivalents (Figure 2B), and the triploid progeny from tetraploid/diploid crosses have six bivalents and six univalents at metaphase I (Figure 2C). The maximum lengths of tetraploid and triploid spindles were not longer than that of diploids, but the spindles were wider, as indicated by the lower aspect ratio at any spindle length (Figure 2E). Rotated tetraploid and triploid spindles were observed with lengths greater than ever observed for diploid spindles, but these rotated spindles still had aspect ratios of ≤1.0 (Figure 2, E and F). *P. typica* was reported to have a genome size 2.7 times greater than that of *C. elegans* (Fleming *et al.*, 2000). Like *C. elegans*, *P. typica* has six bivalents at metaphase I (Figure 2D), but the volume of each bivalent was 2.4 times greater than that of a *C. elegans* bivalent (*P. typica*, 5.5 ± 0.2 μm^3, $n = 12$; *C. elegans*, 2.3 ± 0.2 μm^3, $n = 7$). The maximum length of *P. typica* meiotic spindles was nearly twice that of those of *C. elegans*, but they still initiated rotation at an aspect ratio of ≤1.0 (Figure 2E). Using the combined data (112 spindles) from diploid, triploid, and tetraploid *C. elegans* and *P. typica* but excluding spindles with ambiguous or intermediate

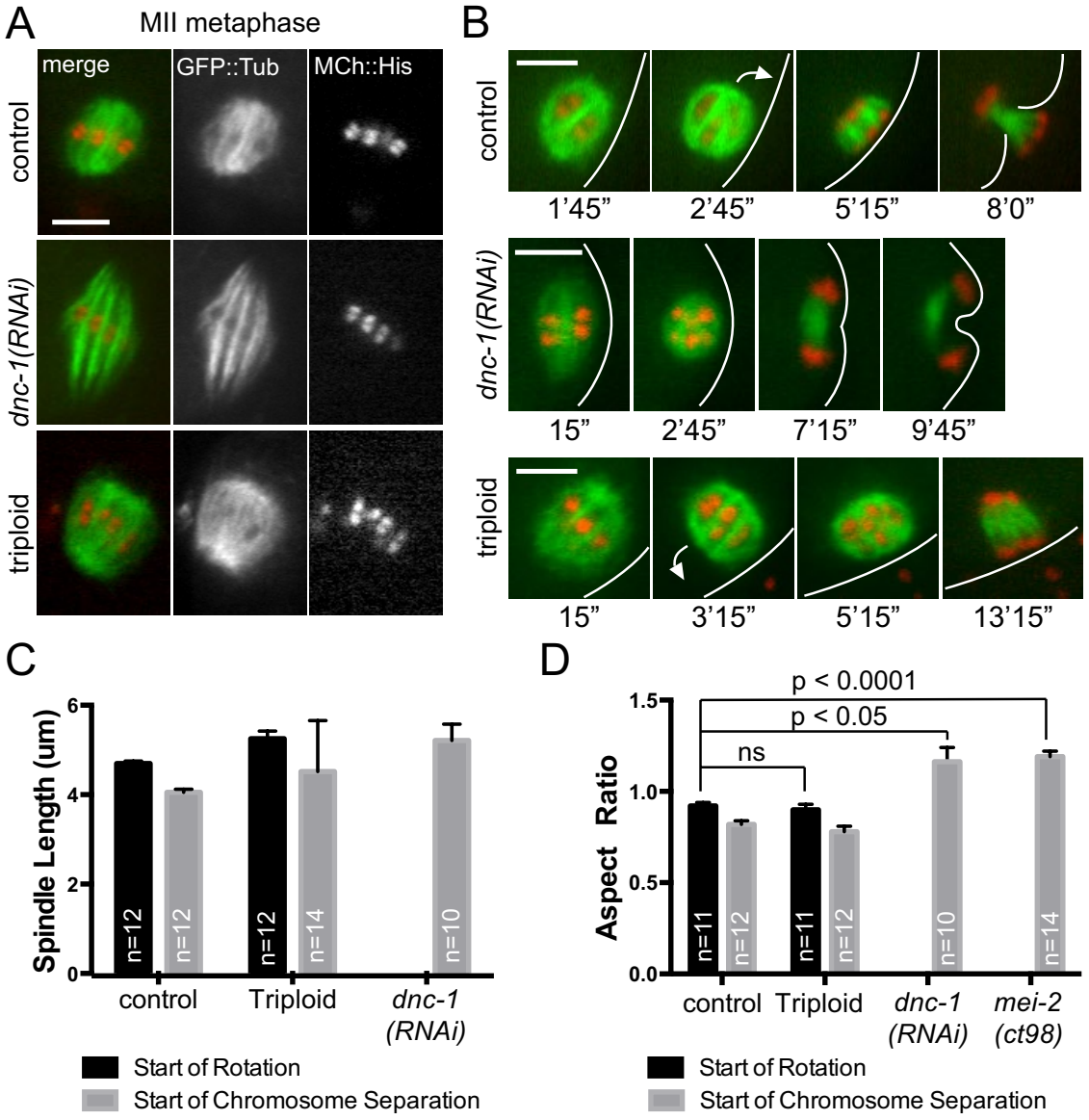

FIGURE 3: Depletion of the dynactin subunit DNC-1 alters spindle length and shape and prevents spindle rotation. (A) Representative images from time-lapse sequences of embryos expressing GFP:tubulin (green) and mCherry:histone H2B (red) showing the different lengths and shapes of control, *dnc-1(RNAi)*, and triploid metaphase spindles. (B) Representative time-lapse sequences of meiosis I embryos showing spindle shape at rotation for control (diploid) and triploid spindles and an example of rotation failure in a *dnc-1(RNAi)* embryo that achieves a spherical spindle shape. Times are from metaphase I. Cortices are indicated by white lines, and arrows indicate the directions of rotation for control and triploid spindles. (C) Quantification of average spindle length from time-lapse sequences. (D) Quantification of average aspect ratio from time-lapse sequences. Bars, 5 μm.

rotation status, we calculated a correlation coefficient of 0.80 for aspect ratio to rotated/not rotated status and a correlation coefficient of 0.66 for spindle length to rotated/not rotated status (Figure 2F). The correlation between aspect ratio and rotation status was significantly better than the correlation between spindle length and rotation status ($p = 0.02$, Fisher *r*-to-*z* transformation and two-tailed *t* test from a *z* score). These results establish a strong correlation between spindle rotation and a nearly spherical spindle shape.

p150 dynactin is required independently for both spherical spindle shape and spindle rotation

We previously reported that depletion of dynein heavy chain by RNAi completely blocked spindle rotation (Ellefson and McNally, 2009), whereas depletion of the dynactin subunit DNC-1 caused only a delay in spindle rotation (Ellefson and McNally, 2011). Using a longer *dnc-1* RNAi feeding regime, we found that spindle rotation completely failed in 19 of 23 embryos expressing mCherry:histone and either GFP:tubulin or GFP:DHC-1. At this degree of DNC-1 depletion, however, we observed significant effects on spindle length and shape. At metaphase, *dnc-1(RNAi)* spindles were composed of microtubule bundles that did not bend inward and join together at the poles, giving the poles a more pointed appearance (Figure 3A), and metaphase spindles were longer than control spindles (*dnc-1(RNAi)* MI, 10.7 ± 0.8 μm, $n = 4$; MII, 9.0 ± 0.4 μm, $n = 5$; control MI, 8.3 μm, MII, 6.9 μm; McNally and McNally, 2011). *dnc-1(RNAi)* spindles shortened like control spindles (Figure 3B) but

were on average longer than the control at the initiation of chromosome separation (Figure 3C). As a result, *dnc-1(RNAi)* spindles had an average aspect ratio >1.0 at chromosome separation (Figure 3D), whereas both control diploid and triploid spindles, which rotated normally, had an aspect ratio <1.0 at the start of rotation. *mei-2(ct98)* is a partial-loss-of-function allele of the regulatory subunit of the microtubule-severing protein katanin. *mei-2(ct98)* spindles do not rotate (McNally *et al*., 2006) and also had an aspect ratio >1.0 at chromosome separation (Figure 3D), supporting the idea that meiotic spindles must achieve a nearly spherical shape to initiate rotation. DNC-1, however, likely has an additional role in spindle rotation because for a subset (5 of 10) of *dnc-1(RNAi)* spindles that did not rotate (Figure 3B), an aspect ratio <1.0 was achieved by chromosome separation and was not significantly different from that of the control ($p = 0.24$). These results support a model in which both spherical spindle shape and a distinct dynein/dynactin activity are required for spindle rotation.

Dynein heavy chain accumulates on the embryo cortex just before initiation of spindle rotation in a dynactin-dependent manner

The majority of proposed dynein-dependent spindle-positioning mechanisms involve cortical dynein pulling on the plus ends of astral microtubules that extend from the spindle to the cortex (Kotak and Gonczy, 2013; Lu and Johnston, 2013; McNally, 2013). Previously we reported accumulation of dynein around the entire cortex of metaphase I–arrested embryos treated with the CDK-1 inhibitor PA (Ellefson and McNally, 2011), but we were unable to reproducibly image cortical dynein during wild-type meiotic spindle rotation (Ellefson and McNally, 2009). Using improved spinning-disk confocal microscopy, we report that 12 of 12 time-lapse sequences of wild-type embryos expressing GFP::dynein heavy chain exhibited accumulation of cortical dynein around most of the exposed embryo (Figure 4A). Because imaging was done in utero, where embryos often overlap each other, measurements were made along the clearest 15- to 20-µm stretch of cortex (Figure 4B). Plotting the ratio of cortical GFP fluorescence to the fluorescence of the adjacent cytoplasm revealed that cortical dynein begins accumulating just before initiation of spindle rotation (Figure 4D). No accumulation of dynein on the cortex or spindle was observed in time-lapse sequences of 12 of 12 *dnc-1(RNAi)* embryos (Figure 4, C, E, and F). Thus DNC-1 is required for spindle rotation (Figure 3B) and for DHC-1 accumulation on both the cortex and spindle. Depletion of GPR-1,2, which are required for mitotic spindle positioning in the one-cell embryo (Colombo *et al*., 2003; Gotta *et al*., 2003; Srinivasan *et al*., 2003) but not meiotic spindle rotation (van der Voet *et al*., 2009), caused a partial reduction in cortical dynein accumulation (Figure 4F). These results show a correlation between spindle rotation and cortical dynein.

We previously reported evidence for microtubules with plus ends extending inward from the cortex (McNally *et al*., 2010). To test whether cortical accumulation of dynein might be due to activation of dynein motility and motoring of the protein toward minus ends at the cortex, we analyzed cortical dynein in tubulin-depleted embryos. For this experiment, we used PA to induce cortical dynein accumulation in metaphase 1–arrested, APC-depleted embryos as described previously (Figure 5, A–D; Ellefson and McNally, 2011). Depletion of the TBA-1 α-tubulin by RNAi completely eliminated the cytoplasmic microtubule array (compare Figure 5, A and E) but only partially reduced PA-induced accumulation of cortical dynein (Figure 5, D, H, and M). The reduced amount of cortical dynein in *tba-1(RNAi)* plus PA compared with control might indicate that a portion of cortical dynein accumulation is due to transport on microtubules or might be due to competition with dynein-coated cytoplasmic filaments that only accumulated in this triple-mutant situation (Figure 5H). Because complete elimination of cytoplasmic microtubules was observed, this result indicates that at least a portion of cortical dynein accumulates due to binding a cortical anchor rather than transport to the cortex on microtubules. Consistent with binding of dynein to a cortical anchor, all cortical dynein accumulation was dependent on LIN-5 (Figure 5, L and M), a cortical anchor for dynein during mitosis (Nguyen-Ngoc *et al*., 2007). LIN-5 is also required for meiotic spindle rotation and accumulation of dynein on the meiotic spindle (van der Voet *et al*., 2009). These results provide additional correlations between spindle rotation and cortical dynein.

Microtubules extend from acentriolar meiotic spindles with plus ends outward during spindle rotation

The majority of proposed dynein-dependent spindle positioning mechanisms involve astral microtubules that have minus ends anchored in the centriole-containing centrosomes at spindle poles and plus ends extending outward toward the cortical dynein. *C. elegans* female meiotic spindles, however, do not have centriole-containing centrosomes at their poles (Albertson and Thomson, 1993), and astral microtubules have been difficult to document (Ellefson and McNally, 2009). Here we report that five of five GFP:tubulin-expressing embryos closest to the objective during in utero imaging had microtubules radiating outward in all directions during spindle rotation (Figure 6A). To determine whether these microtubules had plus ends radiating outward, we captured time-lapse images of *C. elegans* embryos expressing GFP:EBP-1. EBP-1 is one of two EB1 (microtubule plus end–binding protein) homologues in *C. elegans* (Srayko *et al*., 2005; Motegi *et al*., 2006). In five of five EBP-1:GFP-expressing embryos closest to the objective during in utero imaging, microtubule plus ends moved outward in all directions from the spindle during rotation (Figure 6B and Supplemental Videos S1 and S2). In one 50-s time-lapse sequence, 29 EBP-1 comets moved outward from the spindle, whereas only 4 moved inward toward the spindle (Supplemental Video S2). These results demonstrate the existence of microtubules extending plus end outward during rotation and in all directions from the spindle, including toward the cortex.

In the most simplistic cortical pulling model, dynein would be enriched at the point on the cortex toward which one spindle pole moves. In eight of 12 time-lapse sequences of GFP-DHC-1–expressing embryos, however, dynein accumulated on the cortex around most of the embryo just before rotation but was not detectable on the cortex immediately adjacent to the spindle until after completion of rotation (Figure 4A and Figure 6C). In the remaining four of 12 control embryos, cortical dynein accumulation was observed adjacent to the spindle before rotation. To test whether the zone of reduced dynein concentration on the cortex is associated with spindle proximity, we analyzed GFP:DHC-1 localization in *kca-1(RNAi)* embryos. In *kca-1(RNAi)* embryos, spindles assemble far from the cortex, then move in a dynein-dependent, APC-dependent, and pole-first manner to the cortex (Yang *et al*., 2005; Ellefson and McNally, 2009, 2011). In five of five *kca-1(RNAi)* embryos, spindles moved toward a cortex that was uniformly labeled with GFP:DHC-1 (Figure 6D). The difference in the fraction of embryos exhibiting a dynein-free patch between control and *kca-1(RNAi)* was significant ($p = 0.029$, Fisher's exact test). This result indicates that the zone of reduced dynein concentration on the cortex is caused by spindle proximity to the cortex before activation of the APC and recruitment

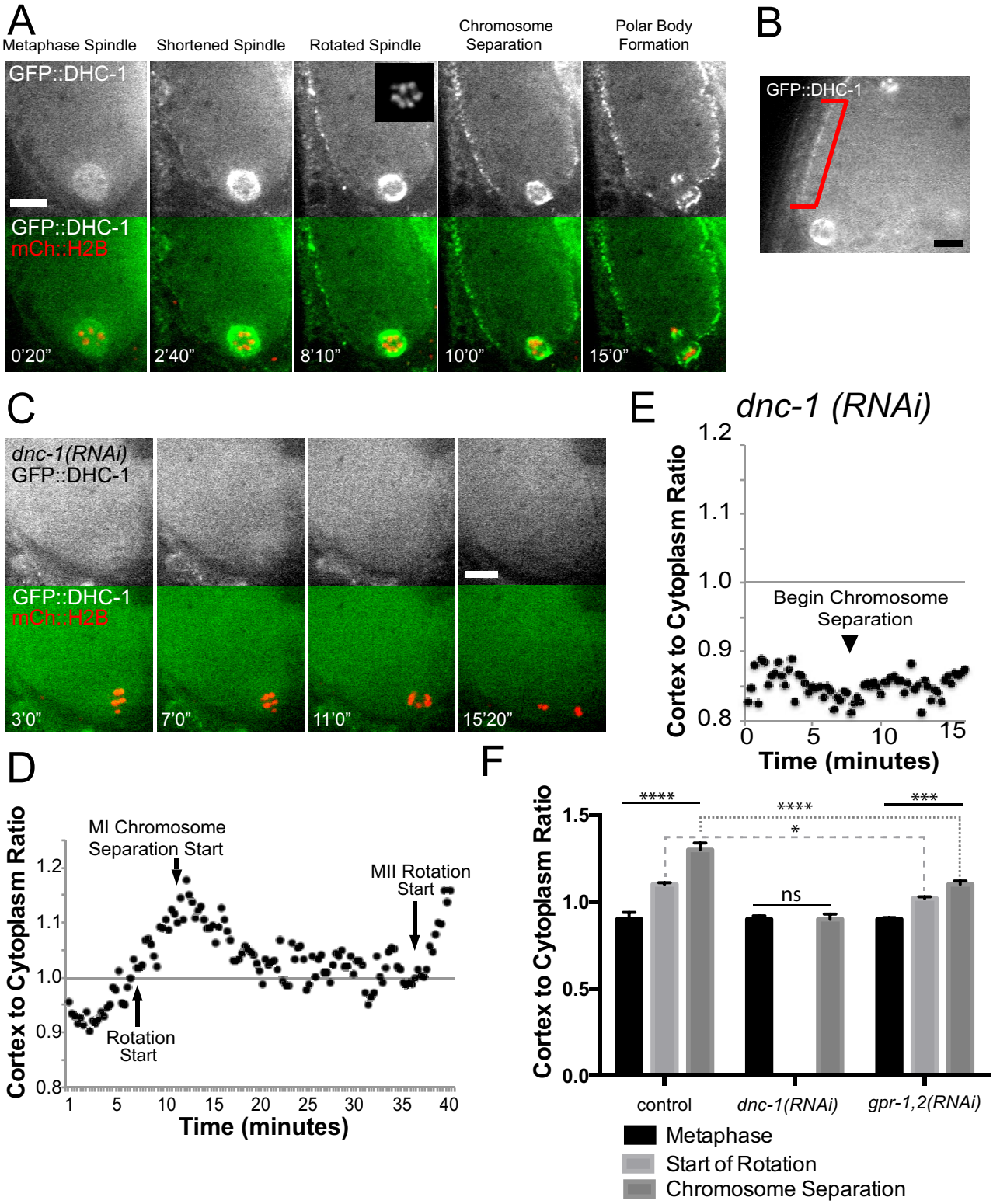

FIGURE 4: Dynactin-dependent cortical dynein heavy chain accumulates just before initiation of spindle rotation. (A) Time-lapse images of a control strain expressing GFP::DHC-1 and mCherry::histone. Times are from spermatheca exit. Punctate cortical dynein is obvious at 8 min, 10 s. (B) Example of a segment of cortex used for quantifying the average pixel value of cortical GFP/cytoplasmic GFP is marked in red. (C) Time-lapse sequence showing no cortical or spindle-associated dynein (GFP:DHC-1) in a *dnc-1(RNAi)* embryo. Chromosomes labeled with mCherry:histone separate parallel to the cortex with no spindle rotation. Times are from spermatheca exit. (D) The ratio of cortical GFP:DHC-1 fluorescence/cytoplasmic fluorescence of the adjacent cytoplasm for a 15-µm stretch of cortex was plotted over time for a representative control embryo and a representative *dnc-1(RNAi)* embryo (E). Times are from metaphase I. (F) The average ratio of cortical GFP:DHC-1 fluorescence/cytoplasmic fluorescence of the adjacent cytoplasm at metaphase, rotation onset, and initiation of chromosome separation from multiple time-lapse sequences. *$p < 0.05$, ***$p < 0.001$, ****$p < 0.0001$. Bars, 5 µm.

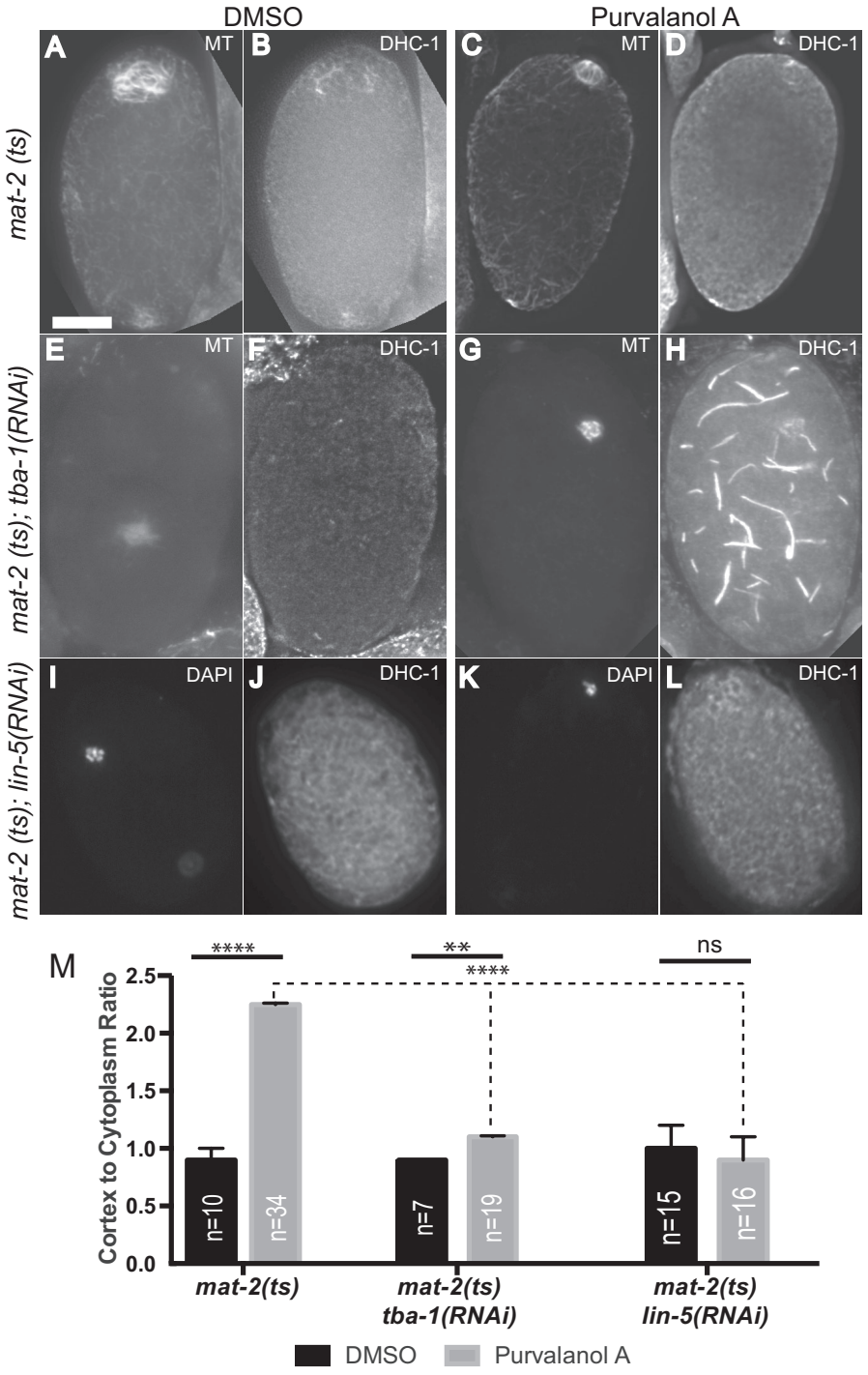

FIGURE 5: Dynein recruitment to the cortex is microtubule independent but LIN-5 dependent. (A, B) *mat-2(ts)* GFP:DHC-1 embryos grown at restrictive temperature for 24 h, dissected into DMSO, fixed, and stained with anti-tubulin antibodies. (C, D) *mat-2(ts)* GFP:DHC-1 embryos grown at restrictive temperature for 24 h, dissected into PA, fixed, and stained with anti-tubulin antibodies. (E, F) Same as A and B, but in embryos also depleted for tubulin using *tba-1(RNAi).* (G, H) Same as C and D, but in embryos also depleted for tubulin using *tba-1(RNAi).* (I, J) Same as A and B, but also depleted of LIN-5 and stained with DAPI. (K, L) Same as C and D, but also depleted of LIN-5 and stained with DAPI. (M) Ratio of cortical dynein intensity to cytoplasmic dynein intensity measured in control embryos and embryos soaked in PA. $^{**}p < 0.01$, $^{****}p < 0.0001$. Bar, 10 μm.

of dynein to the cortex. This region of reduced dynein concentration must not be essential for rotation or late translocation since it was not observed in four of 12 control embryos or five of five *kca-1(RNAi)* embryos. One possible explanation is that cortical dynein molecules are removed from the cortex as they motor toward the minus ends of astral microtubules after exerting a transient pulling interaction at the cortex (see *Discussion*).

CDK-1–dependent phosphorylation of the basic domain reduces microtubule association of p150 dynactin

Purvalanol A–mediated inhibition of CDK-1 induces dynein-dependent meiotic spindle rotation in APC-depleted *C. elegans* meiotic embryos (Ellefson and McNally, 2011). This result suggested that spindle rotation is induced by dephosphorylation of a dynein regulator. We focused on the basic, serine-rich domain adjacent to the CAP-Gly domain of the p150 dynactin subunit DNC-1 because this region had a high density of in vivo phosphorylation sites (Bodenmiller *et al.*, 2008; Zielinska *et al.*, 2009), and the CAP-Gly domain is required for movement against high load (Moore *et al.*, 2009). We previously found that PA-mediated inhibition of CDK-1 in metaphase-arrested *Xenopus* A6 cells expressing GFP-tagged *C. elegans* DNC-1 N-terminus (amino acids [aa] 1–193) caused increased microtubule association of the DNC-1 N-terminal microtubule-binding domain, thereby demonstrating that CDK-1 inhibits the microtubule association of DNC-1 (Ellefson and McNally, 2011). This could result from the reversal of inhibitory phosphorylations on the basic, serine-rich domain that would increase the microtubule-binding affinity of the adjacent CAP-Gly domain. Alternatively, CDK-1–mediated inhibition could result in removal of an unknown protein from the spindle that allows DNC-1 to access spindle microtubules.

To test whether direct phosphorylation of the basic domain of DNC-1 inhibits microtubule interactions, we made expression constructs of the *C. elegans* DNC-1 N-terminus that contained the CAP-Gly/microtubule-binding domain (aa 5–69; Waterman-Storer *et al.*, 1995; Weisbrich *et al.*, 2007) and the basic domain (aa 70–272; Culver-Hanlon *et al.*, 2006; Kincaid and King, 2006), fused to GFP (Figure 7B). A nonphosphorylatable (7S>A) version had seven in vivo–phosphorylated serines (Bodenmiller *et al.*, 2008; Zielinska *et al.*, 2009) changed to alanine, and a phosphomimetic (7S>E) version had the same residues changed to glutamate. Each construct was transfected into *Xenopus* A6 cells. Cells were then arrested in metaphase with the proteasome inhibitor MG132 and then treated with either dimethyl sulfoxide (DMSO) as a solvent control or the CDK-1 inhibitor PA

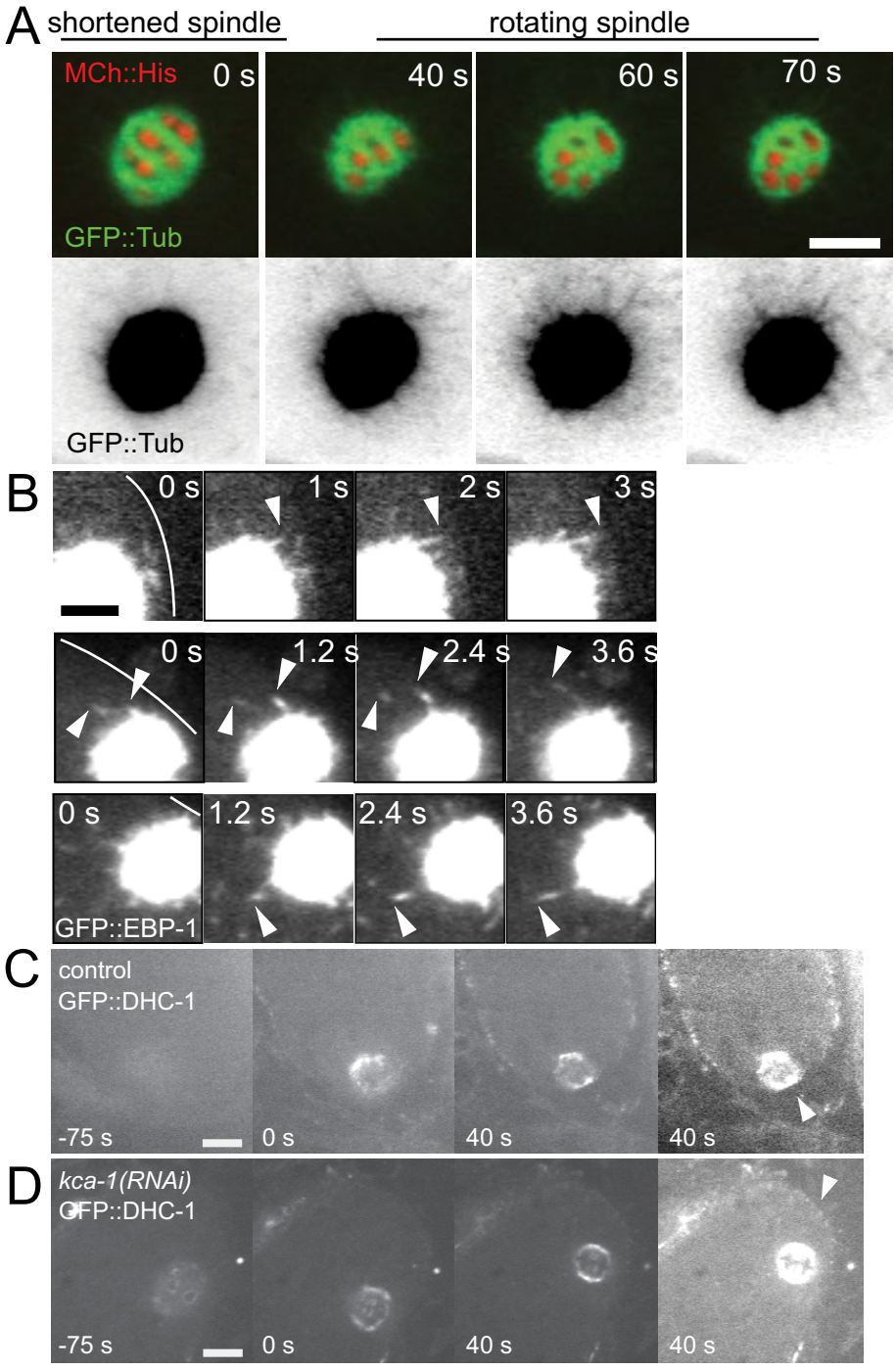

FIGURE 6: Astral microtubules extend from acentriolar spindles. (A) Time-lapse images of a shortened meiotic spindle near the upper surface of an embryo reveal microtubules that extend toward the cytoplasm. The microtubules emanate from both the spindle poles and the nonpolar regions. Because the spindle is positioned at the upper cortex, rotation occurs into the plane of focus. Indicated times are relative to the start of rotation. Bar, 4 μm. (B) EBP-1 comets extend outward from shortened meiotic spindles. Images of embryos expressing GFP::EBP-1 were captured at 1.0- or 1.2-s intervals. Arrowheads indicate the leading edge of comets traveling outward from the spindle. Lines indicate the position of cortices. Two of the comets extend to the cortex. Bar, 3 μm. (C) Representative images from a time-lapse sequences of embryos expressing GFP::DHC-1 in a control background and (D) *kca-1(RNAi)*. Time 0 represents the first frame after rotation in wild type or initiation of movement toward the cortex in *kca-1(RNAi)*. Arrowheads indicate where the spindle contacts the cortex. Bar, 5 μm.

(Villerbu *et al.*, 2002; Goga *et al.*, 2007). To quantify DNC-1(1-272):GFP signal levels while controlling for cell-to-cell differences in protein expression, we measured the average pixel intensity of DNC-1(1-272):GFP on spindle microtubules/centrosomes as a ratio to cytoplasmic DNC-1(1-272):GFP. In metaphase-arrested control cells, wild-type DNC-1(1-272):GFP localized to centrosomes and was faintly detected on the mitotic spindle (Figure 7D). Inhibition of CDK-1 resulted in a significant increase in the wild-type DNC-1(1-272):GFP signal on spindle and astral microtubules (Figure 7, E and L, and Supplemental Table S1). These results recapitulate our previous findings that inhibition of CDK-1 increases the microtubule association of p150's MT-binding domain (Ellefson and McNally, 2011). In DMSO-treated, metaphase-arrested cells where CDK-1 is active, nonphosphorylatable DNC-1(7S>A, 1-272):GFP was significantly enriched on spindle and astral microtubules when compared with wild-type DNC-1(1-272):GFP (Figure 7, F and L). Inhibition of CDK-1 did not alter or increase the spindle and astral microtubule enrichment of DNC-1(7S>A, 1-272):GFP (Figure 8, G and L, and Supplemental Table S1). Conversely, phosphomimetic DNC-1(7S>E, 1-272):GFP was not enriched on spindle or astral microtubules in both DMSO-treated and PA-treated, metaphase-arrested cells (Figure 7L and Supplemental Figure S3). We did not observe any significant changes in the ratio of anti-tubulin staining of the spindle relative to the cytoplasm (Supplemental Table S2). Wild-type, phosphomimetic, and nonphosphorylatable DNC-1(1-272):GFP in interphase cells all localized similarly along the lengths of microtubules, regardless of CDK-1 inhibition (Supplemental Figure S2). This result suggests that phospho-dependent changes of DNC-1 N-terminal microtubule association are specific to M phase. These results support a model in which APC-dependent recruitment of dynactin to spindle microtubules is mediated by dephosphorylation of the basic domain of DNC-1.

The CAP-Gly domain is required for phosphoregulation of p150 microtubule association.

p150 CAP-Gly and basic domains have each been reported as sufficient to bind microtubules (Culver-Hanlon *et al.*, 2006). To determine whether the basic domain alone is sufficient for displaying phospho-dependent changes in microtubule association, we

generated truncated "basic" DNC-1(70-272):GFP expression constructs that no longer contained the CAP-Gly domain (Figure 7C). We analyzed the localization of wild-type, 7S>A, and 7S>E DNC-1(70-272):GFP in MG132-arrested *Xenopus* A6 treated with DMSO or PA. We observed very little association of any of the basic-domain-only constructs with spindle microtubules, and there was no significant change upon treatment with PA (Figure 7L, Supplemental Figure S3, and Supplemental Table S3). Because no phosphorylation sites have been reported in the CAP-Gly domain itself (Bodenmiller *et al.*, 2008; Zielinska *et al.*, 2009), our results suggest that p150 microtubule association requires the CAP-Gly domain but can be regulated through phosphorylation of the adjacent basic domain.

Nonspecific electrostatic interactions adjacent to the CAP-Gly domain mediate microtubule association

Dephosphorylation of the basic domain might increase microtubule-binding affinity of the adjacent CAP-Gly domain by influencing allosteric interactions between the CAP-Gly domain, the basic domain, and the microtubule. Alternatively, dephosphorylation of the basic domain might simply increase the net positive charge of an unstructured region next to the CAP-Gly domain. To distinguish between these possibilities, we generated DNC-1(1-75+Synthetic):GFP expression constructs that contain the DNC-1 CAP-Gly domain and replaced the basic domain with a synthetic 47-aa peptide fused to GFP (Figure 8A). The synthetic 47-aa peptide contained no phosphorylatable amino acids and had no homology with the native basic domain. Four DNC-1(1-75:+Synthetic):GFP expression constructs were made that differed at specific positions to contain either a basic (K/R) or acidic (D/E) amino acid that cumulatively generated a differing net charge (+14, +7, +0, –7) for each synthetic peptide. We analyzed the localization of DNC-1(1-75:+Synthetic):GFP in MG132-arrested *Xenopus* A6 cells treated with DMSO (Figure 8, B–G). DNC-1(1-75: +14):GFP showed the strongest localization to spindle microtubules (n = 8), most similar to DNC-1(7S>A,1-272):GFP (n = 8; Figure 8, C and G). DNC-1(1-75: +7):GFP also associated with spindle microtubules but to a lesser extent (n = 12; Figure 8, D and G). Conversely, both DNC-1(1-75: +0):GFP (n-9) and DNC-1(1-75: -7):GFP (n = 9) did not strongly associate with spindle microtubules (Figure 8, E–G). We also observed charge-dependent microtubule association in interphase cells. Both DNC-1(1-75: +14):GFP (n = 10) and DNC-1(1-75: +7):GFP (n = 8) localized along the entire lengths of interphase microtubules (Figure 8, I and J), which was also seen for the full-length (aa 1–272) p150 N-terminal microtubule-binding domain, regardless of phosphorylation state (Supplemental Figure S2). Conversely, DNC-1(1-75: +0):GFP (n = 11) and DNC-1(1-75: -7):GFP (n = 8) did not localize to interphase microtubules (Figure 8, K and L). Together, these results suggest that the nonspecific positive charge in the peptide region adjacent to the CAP-Gly domain promotes microtubule association. These results also suggest that the number of phosphorylated residues, rather than the identity of the phosphorylated residues, is important for modulating microtubule association in vivo during M phase.

The *C. elegans* p150 basic domain is phosphorylated in vitro in a purvalanol-sensitive manner

The reported in vivo phosphorylation sites in the DNC-1 basic domain (Bodenmiller *et al.*, 2008; Zielinska *et al.*, 2009) were determined from mixed-stage *C. elegans*, and thus it is not known whether these sites would be phosphorylated during metaphase of meiosis I and meiosis II. Because we could not isolate *C. elegans* meiotic metaphase extracts that maintained their phosphorylation state, and because the sequence of the basic domain is not conserved, we analyzed in vitro phosphorylation sites generated on *Escherichia coli*–expressed and purified *C. elegans* DNC-1 CAP-Gly plus basic domains that were incubated either with purified cyclin B/CDK-1 or extracts prepared from metaphase I *Spisula solidisima* oocytes. Two phosphosites, Ser-111 and Ser-268, that were previously identified in vivo (Bodenmiller *et al.*, 2008; Zielinska *et al.*, 2009) were identified as purvalanol-sensitive sites generated in vitro by both purified cyclin B/CDK-1 and *Spisula* oocyte extract (Table 1). One additional purvalanol-sensitive phosphosite, Ser-271, was generated by both cyclin B/CDK-1 and *Spisula* extract but was not previously identified in vivo. These three sites correlate most strongly with our in vivo observations of purvalanol-induced spindle rotation. A combined total of 13 phosphosites were identified in vitro (this study) and in vivo (Bodenmiller *et al.*, 2008; Zielinska *et al.*, 2009), all in the basic domain and none in the CAP-Gly domain. The basic domain would have a net charge of +13 in the completely dephosphorylated state, and phosphorylation of 13 serines would reduce the charge to neutral. The results shown in Figure 8 indicate that a range of net charges from +13 to neutral would be sufficient to drive DNC-1 from mostly bound to mostly unbound to microtubules. These results support a model in which the timing of meiotic spindle rotation is modulated by the phosphorylation state of the DNC-1 basic domain.

DISCUSSION

Spindle positioning through a cortical pulling mechanism requires cortically anchored dynein and astral microtubules with plus ends extending to the cortical motors. Here we demonstrate that during *C. elegans* female meiotic spindle rotation, dynein is present on the cortex, and microtubule plus ends grow outward from the spindle to the cortex. We also demonstrate that dynactin is required for both cortical dynein accumulation and meiotic spindle rotation. These results strongly support a dynein/dynactin-dependent cortical pulling mechanism for *C. elegans* meiotic spindle rotation.

Meiotic spindles, in a subset of dynactin-depleted embryos, had near wild-type length and width when they failed to rotate. This result is consistent with a direct role for dynactin in cortical pulling by dynein. More penetrant dynactin depletion, however, also altered spindle length and shape. Altered spindle shape has also been observed in other genotypes that prevent spindle rotation (*dhc-1(RNAi or ts)*, *aspm-1(RNAi or ts)*, *mei-2(ct98)*; McNally *et al.*, 2006; Ellefson and McNally, 2009; van der Voet *et al.*, 2009; Connolly *et al.*, 2014). In embryos with these genotypes, spindles are more elongated than wild-type spindles, which are nearly spherical when they rotate. Our analysis of spindle length and aspect ratio of prerotation and postrotation spindles in situations with altered spindle scaling demonstrates a strong correlation between spherical shape and rotation. This correlation might be coincidental, or it might suggest that either spindle rotation causes spherical spindle shape or spherical shape facilitates rotation. It is unlikely that rotation causes spherical shape, because spindles can achieve spherical shape in the absence of rotation (Figure 3B; Ellefson and McNally, 2009). A spherical spindle can rotate around an axis without moving through any new cytoplasm, and thus its movement is not opposed by the elastic properties of cytoplasm. In contrast, rotation of a prolate ellipsoid around its minor axis would be opposed by the elastic properties of the cytoplasm. At high frequencies, the Young's modulus of cytoplasm has been found to be much higher than that of an 80 μM solution of F-actin and more similar to that of a solution of F-actin cross-linked

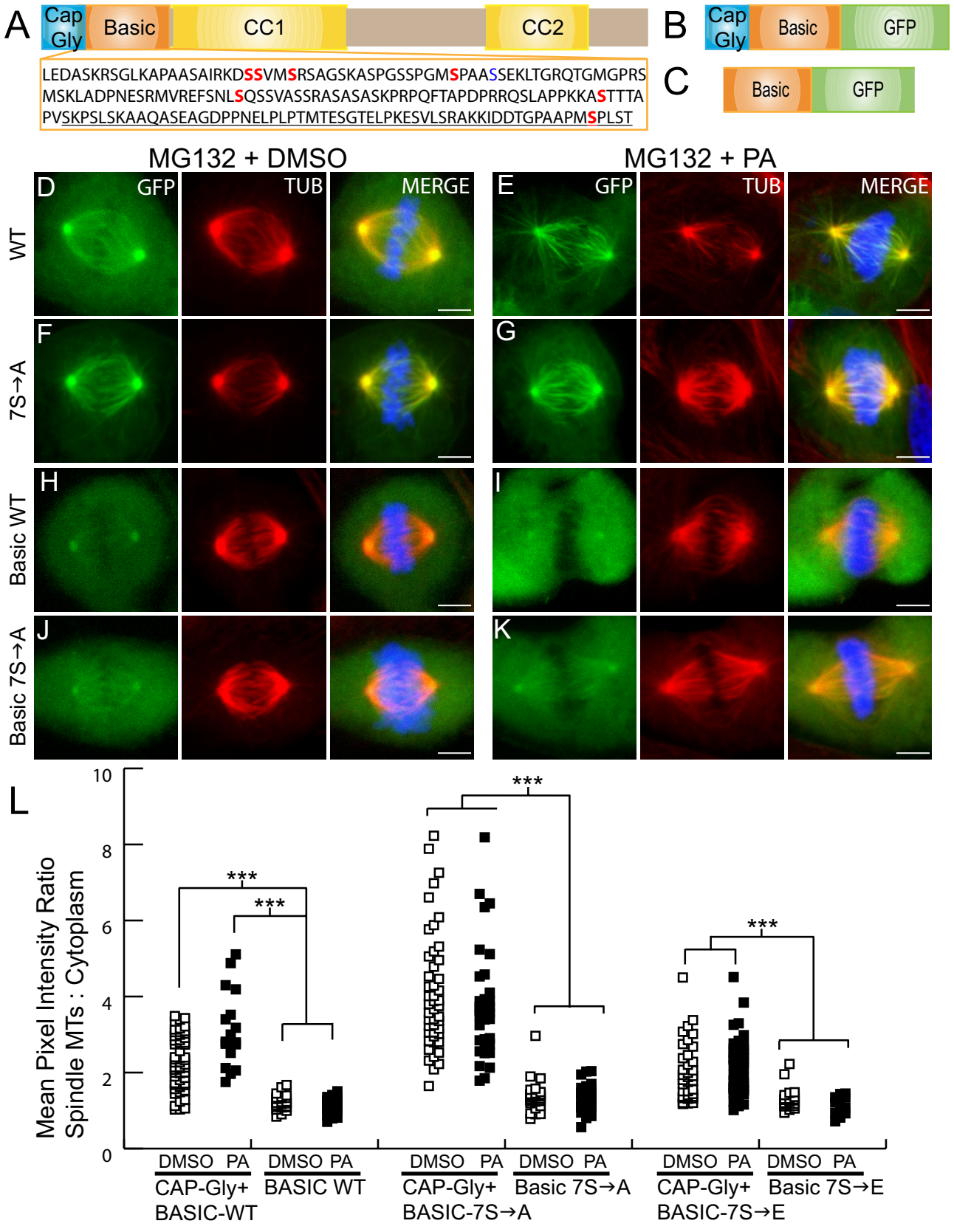

FIGURE 7: Phosphorylation of the basic domain decreases microtubule association of the DNC-1 N-terminal microtubule-binding domain. (A) Schematic of *C. elegans* p150 (DNC-1) highlighting the sequence of the basic domain contained in the expression constructs. Identified in vivo phosphorylation sites (red) were mutated to Ala or to Glu in transfection constructs. The underlined sequence indicates amino acids included in the constructs used that were not included in previously reported experiments. (B) Schematic of the *C. elegans* DNC-1 N-terminal CAP-Gly plus basic

by α-actinin (Wachsstock *et al.*, 1993; Yamada *et al.*, 2000). Spindle rotation occurs at very low frequency, and Young's moduli have been measured for actin and actin/α-actinin gels at very low frequency (Wachsstock *et al.*, 1993; Xu *et al.*, 1998). Using a Young's modulus of 1 pN/μm^2 as an approximation for the elasticity of cytoplasm at low frequency, an ellipsoid metaphase spindle undergoing a 90° rotation could encounter ~18 pN of resistance due to the elastic nature of the surrounding cytoplasm, whereas the sphere would encounter zero elastic resistance. The timing of late translocation in *kca-1(RNAi)* embryos and the occasional straight rotation (Supplemental Figure S1) could not be explained by the ability of a sphere to rotate within its own volume. In these cases, even a spherical spindle would encounter both frictional drag and resistance from the elasticity of the cytoplasm, and the reduction in spindle volume might be more important than the change in shape.

An unusual feature of *C. elegans* meiotic spindle rotation is the failure of dynein to accumulate on the cortex near the spindle until long after completion of rotation in a subset of embryos. During mitosis, astral microtubule plus ends make transient contacts with the cortex that last only 1 s on average (Kozlowski *et al.*, 2007). We suggest that these transient cortical pulling interactions frequently terminate as cortical dynein molecules release from the cortex and motor toward the microtubule minus ends in the spindle. Early in the wild-type rotation cycle, the rate of dynein recruitment to the cortex might be low due to incomplete dephosphorylation of CDK substrates. The close proximity of the metaphase spindle would result in a high density of astral microtubule plus ends contacting the cortex and thus a high rate of removal of dynein from the cortex. The combination of slow recruitment and fast removal could generate the apparent dynein-free zone observed during rotation. Later in the cell cycle, the rate of dynein recruitment to the cortical anchor might be higher due to more complete dephosphorylation of CDK substrates, resulting in eventual recruitment of dynein to the cortex adjacent to the spindle (Figure 4A, 15 min). A dynein-free zone was not observed in 5/5 *kca-1(RNAi)* embryos. In *kca-1(RNAi)*, the spindle is far from the cortex early in the cell cycle, so the rate of dynein removal would be slow due to the low density of astral microtubule contacts. By the time the spindle reaches the cortex in *kca-1(RNAi)* embryos, the rate of dynein recruitment would be high because it is later in the cell cycle. Thus, in *kca-1(RNAi)* embryos, the rate of dynein removal may never be higher than the rate of dynein recruitment at the cortex. Depletion of cortical dynein due to close proximity of the mitotic spindle has been reported in HeLa cells (Kiyomitsu and Cheeseman, 2013). In HeLa cells, however, localized depletion of cortical dynein results in movement away from the depleted cortex because the astral microtubules extending from the opposite spindle pole can reach the opposite cortex. In contrast, *C. elegans* meiotic spindle poles remain tightly juxtaposed against the cortex, and it is unlikely that astral microtubules from the opposite spindle pole can reach the opposite cortex.

The induction of dynein-dependent spindle rotation by CDK-1 inhibition (Ellefson and McNally, 2011) indicates that cortical pulling by dynein is somehow activated by dephosphorylation after APC-dependent inactivation of cyclin B/CDK-1. Depletion of dynein or dynactin, however, causes spindle length and shape defects before APC activation. Thus dynein/dynactin must be active during metaphase in wild-type embryos. Therefore APC-dependent dephosphorylation must activate some specific property of dynein/dynactin that is required for rotating the spindle. The microtubule-binding CAP-Gly domain of p150 dynactin is not required for dynein motility or processivity (Kardon *et al.*, 2009) but is required in vivo for dynein to pull a nucleus against significant resistance (Moore *et al.*, 2009). Our results indicate that during metaphase, phosphorylation of the basic domain adjacent to the DNC-1 CAP-Gly domain inhibits microtubule binding through a charge neutralization mechanism. APC-dependent inactivation of cyclin B/CDK-1 results in dephosphorylation of the basic domain. This dephosphorylation restores the net positive charge of the basic domain, allowing it to interact with the negatively charged tails of α- and β-tubulin subunits, thus increasing the overall binding of the CAP-Gly domain to the EEFY motifs of tubulin (Weisbrich *et al.*, 2007). High-affinity binding of the CAP-Gly domain to microtubules would enhance dynein's ability to pull one spindle pole to the cortex by a mechanism that has not yet been elucidated. It is likely that additional proteins are dephosphorylated to promote cortical anchoring by dynein. This pathway is significant because anaphase-specific, dynein-mediated spindle-positioning mechanisms are found in other species (Kiyomitsu and Cheeseman, 2013).

Detailed studies of acentriolar meiotic spindle positioning have been reported only for *C. elegans* and mouse. Whereas acentriolar meiotic spindle rotation in *C. elegans* is actin independent (Yang *et al.*, 2003), rotation of acentriolar meiotic spindles in mouse oocytes is actin dependent (Maro *et al.*, 1984) and myosin II dependent (Wang *et al.*, 2011). In *C. elegans*, spindle rotation completes before chromosome separation and before activation of myosin-dependent cortical invaginations (Fabritius *et al.*, 2011) that mediate polar body extrusion. In contrast, mouse meiosis II spindle rotation occurs after chromosome separation and during myosin-dependent cortical invaginations involved in polar body formation (Wang *et al.*, 2011). It is a reasonable interpretation of time-lapse image sequences (Wang *et al.*, 2011) that rotation of the mouse MII spindle is caused by actomyosin-dependent deformation of the cortex. In contrast, *C. elegans* meiotic spindles rotate in the absence of any cortical deformation (Figure 1A). Thus it will be important to discover how acentriolar spindle rotation occurs in other organisms.

MATERIALS AND METHODS

C. elegans strains

FM125 (*unc-119(ed3); ruIs57[pAZ147:pie-1/β-tubulin::GFP; unc-119(+)]; itIs37 [unc-119(+) pie-1::mCherry::H2B]*), EU1561 (*orIs17 [dhc-1::GFP::DHC-1, unc-119(+)]; itIs37 [unc-119(+) pie-1::mCherry::H2B]*), FM231 (*orIs17 [dhc-1::GFP::DHC-1, unc-119(+)]; itIs37 [unc-119(+) pie-1::mCherry::H2B*]; *him-8(e1489)*), SV935 (*mat-2(ax76ts) II; orIs17 [dhc-1-GFP–DHC-1, unc-119(+)]; itIs37[unc-19(+) pie-1-mCherry–H2B]*), WH327 (*unc-119(ed3); ojIs23 GFP:SP12*), FM143 (*unc-119(ed3); ojIs23 GFP:SP12; itIs37 [unc-119(+)*

domain constructs transfected into *Xenopus* A6 cells where DNC-1(1-272) was fused to GFP. (C) Schematic of the basic only constructs which were fused to GFP. (D–K) Representative images of fixed MG132-treated, metaphase-arrested *Xenopus* A6 cells expressing the indicated CAP-Gly plus BASIC:GFP fusions and treated with DMSO or PA and stained with DAPI and anti-tubulin. (L) Quantification of spindle association of each fusion protein in MG132-treated, metaphase-arrested cells treated with DMSO (open squares) or PA (closed squares). Each data point represents an individual cell. ***$p < 0.0001$. Scale bars, 5 μm.

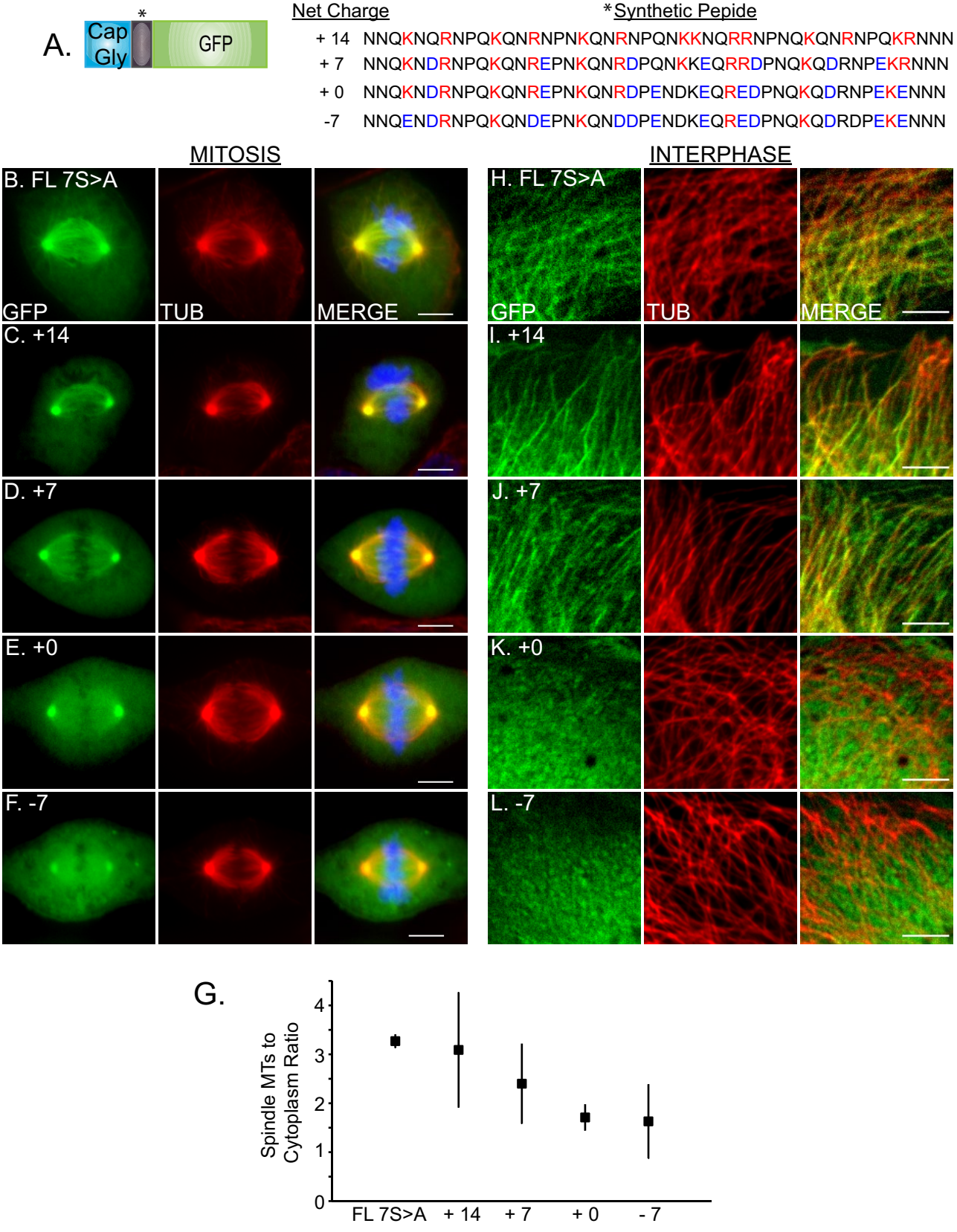

FIGURE 8: Nonspecific electrostatic interactions adjacent to the CAP-Gly domain mediate microtubule association. (A) Schematic of *C. elegans* DNC-1 CAP-Gly plus synthetic peptide constructs fused to GFP and transfected into *Xenopus* A6 cells and sequences of synthetic peptides fused to the CAP-Gly domain with the basic (red) and acidic (blue) amino acid substitutions and the net charge of the synthetic peptides. (B–F) Representative images of fixed, MG132-treated, metaphase-arrested *Xenopus* A6 cells treated with DMSO expressing (B) 7S>A nonphosphorylatable

Kinase	Purvalanol A (10 μM)	Okadaic acid (200 nM)	Phosphosite	MASCOT score	Threshold
Cyclin B/CDK-1			Ser-107	63	18
			Ser-271	58	20
			Ser-111	48	16
			Ser-268	28	19
Cyclin B/CDK-1	+		Ser-187	36	21
Spisula extract			Ser-147	44	25
			Ser-271	58	20
			Ser-111	48	16
			Ser-268	28	19
Spisula extract	+		Ser-147	70	25
Spisula extract		+	Ser-147	57	22
			Ser-107	70	23
			Ser-111	70	23
			Ser-130	42	21
			Ser-92	23	20
			Ser-179	26	21
In vivo (Bodenmiller *et al.*, 2008; Zielinska *et al.*, 2009)			Ser-91		
			Ser 92		
			Ser 95		
			Ser 111		
			Ser 150		
			Ser 187		
			Ser 268		

Phosphorylation sites generated by incubating purified *C. elegans* DNC-1 CAP-Gly plus basic domain with purified cyclin B/CDK-1 or M-phase *Spisula* egg extract.

TABLE 1: In vitro DNC-1 phosphorylation sites.

pie-1::mCherry::H2B]), FM232 (*unc-119(ed3); ruIs57[pAZ147:pie-1/β-tubulin::GFP; unc-119(+)]; itIs37 [unc-119(+) pie-1::mCherry::H2B]; ltIs38 [pAA1; pie-1::GFP::PH(PLC1delta1)+ unc-119(+)]*), and FM287 (*unc-119(ed3); orEx20[mCherry-tba-1 + unc-119(+)]; tjIs8[pie-1:GFP:ebp-1 + unc-119(+)]*) were made by crossing EU1627 and SA141, SP346 (4A, 4X tetraploid), DF5025 (*P. typica* wild isolate).

RNA interference

As described by Timmons *et al.* (2001) and Kamath *et al.* (2001), the RNAi experiments performed were carried out by feeding bacteria (HT115) induced to express double-stranded RNA from L4440 plasmid clones (MRC Gene Services, Source Bioscience, Cambridge, United Kingdom; Kamath *et al.*, 2001), and controls were fed HT115 bacteria transformed with the empty L4440 expression vector. L4 hermaphrodites were transferred to RNAi plates and allowed to feed on the RNAi bacterial lawn for 30–48 h at 25°C.

In utero live imaging

Adult hermaphrodites were anesthetized with tricaine/tetramisole as described (Kirby *et al.*, 1990; McCarter *et al.*, 1999) and gently mounted between a coverslip and a thin 3% agarose pad on a slide. Imaging was carried out as described later.

Immunofluorescence

Meiotic embryos were extruded from hermaphrodites by gentle squishing between coverslip and slide, flash frozen in liquid N_2, permeabilized by removing the coverslip, and then fixed in cold methanol before staining with antibodies and DAPI. Antibodies used in this work were mouse monoclonal anti-tubulin (DM1alpha; 1:200; Sigma-Aldrich), mouse monoclonal DM1alpha: fluorescein isothiocyanate conjugated (1:30; Sigma-Aldrich), rabbit anti-ASPM-1 (1:100; van der Voet *et al.*, 2009), and Alexa 594 anti-rabbit and Alexa 594 anti-mouse (both used at 1:200 and from Molecular Probes).

DNC-1(5-272):GFP as a control, $n = 8$, (C) DNC-1(1-75: +14):GFP, $n = 8$, (D) DNC-1(1-75: +7):GFP, $n = 12$, (E) DNC-1(1-75: +0):GFP, $n = 9$, or (F) DNC-1(1-75: −7):GFP, $n = 9$, stained with DAPI and anti-tubulin. (G) Quantification of the differentially charged DNC-1(1-75: +synthetic):GFP average ratio of the mean pixel intensity of spindle/cytoplasm in MG132 metaphase-arrested cells treated with DMSO. Each data point represents the average ratio, and error bars represent the SD. (H–L) Representative images of fixed interphase *Xenopus* A6 cells treated with DMSO expressing (H) 7S>A nonphosphorylatable DNC-1(5-272):GFP as a control, $n = 10$, (I) DNC-1(1-75: +14):GFP, $n = 10$, (J) DNC-1(1-75: +7):GFP, $n = 9$, (K) DNC-1(1-75: +0):GFP, $n = 11$, or (L) DNC-1(1-75: −7):GFP, $n = 8$, stained with DAPI and anti-tubulin. Scale bars, 5 μm.

Image acquisition and deconvolution

Images from Figures 1A, 2, 5, and 8 were captured on an Olympus IX81 microscope equipped with a 60× PlanApo numerical aperture (NA) 1.42 oil objective and an ORCA Flash 4.0 CMOS camera (Hamamatsu Photonics). Mercury arc excitation light was shuttered by a Sutter Lambda 10-3 shutter controller (Sutter Instruments), and an Olympus disk scanning unit was used for imaging fixed embryos or cells. *Z*-stacks were acquired with 200-nm steps.

Images in Figure 1B were captured on an Intelligent Imaging Innovations Marianas Spinning Disk Confocal equipped with a Photometrics Cascade QuantEM 512SC electron-multiplying charge-coupled device (CCD) and Zeiss 63×/NA 1.4 objective. Image sequences in Figures 3, 4, 6, and 7, Supplemental Figure S1, and supplemental videos were captured with a PerkinElmer-Cetus Ultraview Spinning Disk Confocal equipped with an Orca R2 CCD and an Olympus 60×/NA 1.4 objective. All images in Figures 1 and 2 were deconvolved using Huygens Professional X11 (SVI). Deconvolutions were performed using theoretical point spread functions calculated from the individual parameters for each microscope. Deconvolutions were run up to 40 iterations using CLME restoration.

Spindle aspect ratio calculations

Spindles that appeared to have both poles in focus on the same *z*-section were assumed to be in profile view (with the pole-to-pole axis nearly perfectly flat). These were measured using two-dimensional linear measurements in FIJI (ImageJ; National Institutes of Health, Bethesda, MD). The length was defined as the longest line to bisect the spindle in the pole-to-pole orientation parallel to this axis, and the width was defined as the longest possible line to bisect the spindle parallel to the metaphase plate. Several spindles had the two poles far apart in the *z*-stack, suggesting a nonflat orientation. These spindles were rotated so as to have their pole-to-pole axis aligned to the *x*-axis (angle of 0° relative to the *x*-axis) and were subject to 3D projection on FIJI along the *y*-axis using maximum intensity calculations, a step size of 200 nm, and interpolated sections. These reconstructions were then rotated to the slice where both poles appeared to be parallel to each other, and the length and width measurements were taken as described previously.

C. elegans and *P. typica* chromosome volume calculations

Z-stacks of DAPI-stained chromosomes were acquired on the Olympus IX81 as described. Individual chromosomes with an average signal to average background ratio of ≥4 were selected if they could be distinguished from all other chromosomes in all *z*-sections. Cropped *z*-stacks were then threshold adjusted in FIJI using the Otsu method to produce a stack of black and white images. These stacks were imported into Imaris and subjected to 3D rendering and volume calculations.

Xenopus A6 cells

DNA encoding amino acids 1–272 of *C. elegans* DNC-1 was synthesized by GenScript (Piscataway, NJ) with an *Xba*I site and Kozak consensus at the 5′ end and an *Xho*I site at the 3′ end and first cloned into pUC57. Three sequences were constructed, one corresponding to wild-type DNC-1 amino acid sequence, one with serines 91, 92, 95, 111, 150, 187, and 268 all mutated to alanine (7S>A), and one with serines 91, 92, 95, 111, 150, 187, and 268 all mutated to glutamate (7S>E). The *Xba*I-*Xho*I fragments were each cloned into the pEGFP-N1 vector (Clontech) and confirmed by sequencing. For the basic-only constructs, DNA encoding DNC-1 amino acids 70–272 was PCR amplified from the wild-type, 7S>A, and 7S>E constructs such that the PCR product had a 5′ *Xba*I site and Kozak sequence and a 3′ *Xho*I site. These truncated wild-type, 7S>A, and 7S>E fragments were then each cloned back into pEGFP-N1 vector and confirmed by sequencing. For the CAP-Gly plus synthetic peptide constructs, DNA encoding amino acids 1–75 of DNC-1 was PCR amplified and cloned into pEGFP-N1. Four double-stranded oligos encoding varying net charges of the synthetic peptide (+14, +7, +0, and −7) were synthesized by GenScript with an *Xba*I site and Kozak consensus at the 5′ end and an *Xho*I site at the 3′ end, cloned downstream of the CAP-Gly domain in pEGFP-N1, and confirmed by sequencing.

Xenopus A6 cells (obtained from David Furlow, University of California, Davis, Davis, CA) were grown at 27°C on coverslips in 70% Leibovitz's L15 medium supplemented with 10% fetal bovine serum and penicillin/streptomycin. Cells were transfected with DNC-1(1-272):GFP, DNC-1(70-272), or DNC-1(1-75 + synthetic peptide) expression constructs using Lipofectamine 2000. At 24 h after transfection, the cells were treated with 25 μM MG132 (Calbiochem). After 60 min in MG132, cells were treated for 5 min with 200 μM PA or an equal volume of DMSO as control solvent. The coverslips were fixed in −20°C MeOH and stained with anti-tubulin antibody (DM1α) and DAPI. Cells were imaged on an Olympus IX81 inverted microscope as described earlier.

Quantification of pixel intensity was carried out with iVision software (BioVision Technologies, Exton, PA). A maximum intensity projection of five planes of a *z*-stack for each image was used. The average pixel intensity was measured by drawing a segment over the spindle microtubules and centrosomes or over the cytoplasm. A segment was draw in the image field where no objects were for each image, and the average pixel intensity measured for this segment was subtracted from both the spindle/centrosome and cytoplasm pixel intensity to correct for background. The ratio of average pixel intensity of [(spindle + centrosomes) – background]/(cytoplasm – background) was calculated for each cell.

In vitro phosphorylation of *C. elegans* DNC-1 purified from *E. coli*

DNA encoding the first 293 amino acids of *C. elegans* DNC-1 was cloned as an *Xba*I–*Xho*I fragment into the intein chitin–binding domain fusion vector pTYB2 (New England BioLabs). The pTYB2-DNC-1 plasmid was then transformed into BL21(DE3). Expression of the DNC-1::intein chitin–binding domain (DNC-1::ICBD) was induced for 2 h with 0.4 mM isopropyl-β-D-thiogalactoside at 37°C. The cells were then resuspended in 20 mM 4-(2-hydroxyethyl)-1-piperazineethanesulfonic acid (HEPES), pH 7.5, 500 mM NaCl, 1 mM ethylene glycol tetraacetic acid (EGTA), and protease inhibitors and then lysed using a microfluidizer. The cell debris was pelleted by centrifugation at 8000 RPM for 20 min at 4°C. The supernatant was aliquoted, flash frozen, and stored at −80°C until needed.

An 8-ml amount of supernatant containing DNC-1::ICBD was incubated with 1 ml of Chitin Resin (New England BioLabs) for 20 min at 4°C. The supernatant was then removed, and the resin was washed with 10 ml of 20 mM Na-HEPES, 500 mM NaCl, and 1 mM EGTA, followed by 10 ml of kinase buffer (20 mM 3-(*N*-morpholino)propanesulfonic acid, 25 mM β-glycerophosphate, 5 mM EGTA, 7.5 mM $MgCl_2$, 1 mM sodium orthovandate, 50 μM ATP). The resin was then soaked with *Xenopus* cyclin B/CDK-1 purified from insect cells (McNally *et al.*, 2002) or metaphase I *Spisula* extract (Palazzo and Vogel, 1999) with 1 mM ATP for 20 min at 4°C. The resin was washed with kinase buffer, and DNC-1 was eluted by cleavage of the intein with kinase buffer plus 50 mM dithiothreitol (DTT).

Trypsin digestion of proteins

Recombinant DNC-1 was first incubated with a final concentration of 5.5 mM DTT at 56°C for 45 min to reduce any disulfide bonds. After DTT incubation, alkylation of free thiol groups was carried out by the addition of 10 mM iodoacetamide for 1 h at room temperature in the dark. The resulting solution was then checked for pH, and 1 M ammonium bicarbonate was added until a pH of 8.0 was attained. Trypsin was added to a final enzyme:substrate ratio of 1:50, and digestion was carried out for a minimum of 8 h at 37C. The reaction was then quenched by flash freezing the sample with liquid nitrogen and stored at −80°C until ready for use. Before phosphoenrichment, samples were dried down using a vacuum centrifuge and then reconstituted into 100 µl of 2% acetonitrile supplemented with 0.1% trifluoroacetic acid (TFA). The sample was then cleaned of detergents and salts by application to a C18 TopTip (Glygen, Columbia, MD) according to the manufacturer's instructions.

Enrichment of phosphopeptides via TiO_2

TiO_2 microtips (Glygen) were equilibrated with 10% acetonitrile and 0.1% TFA. To the equilibrated microtip, 100 µmol of reduced, alkylated, and trypsin-digested DNC-1 was applied. Nonphosphorylated peptides were washed away with the equilibration buffer before phosphorylated peptide elution with 200 mM NH_4OH. The elution was then dried down in a vacuum centrifuge before reconstitution in a solution of 2% acetonitrile with 0.1% TFA.

Nano–high-performance liquid chromatography–electrospray ionization tandem mass spectrometry of DNC-1

Mass spectrometry (MS) was performed on an LTQ-Orbitrap XL (Thermo Fisher, San Jose, CA) equipped with an ADVANCE ion max source (Michrom Biosciences, Auburn, CA), a Surveyor MS pump (Thermo Fisher), and a microautosampler (Thermo Fisher). The online column was made of 100 µm–internal diameter fused silica packed in-house with C18 Magic Beads (Michrom Biosciences) with particle size 5 µm in diameter and 0.01-µm pore size. Preequilibration of the column was done with 100% solvent A (0.1% [vol/vol] formic acid in water) for 10 min with subsequent loading of the sample onto the column for 20 min at 2% solvent B (0.1% [vol/vol] formic acid in acetonitrile) at a final flow rate between 500 and 750 nl/min. The gradient used to elute the peptides was as follows, with percentages indicating amount of solvent B: 2–10% for 5 min, 10–35% for 65 min, 35–70% for 5 min, 70–90% for 5 min, and then 2% B for 10 min. The collision energy for the ion trap was set to 35% with resolution at 30,000. The top five most-abundant ions were selected using data-dependent acquisition with a minimum threshold of 55,000 and dynamic exclusion for 60 s, repeat count at 2, repeat duration at 30 s. After acquiring data, the RAW files were converted to MGF files and searched using MASCOT 2.2 (Matrix Science, London, United Kingdom) against an in-house database consisting of 600 proteins, including recombinant DNC-1 and its reversed sequence. Other sequences included common contaminants, including human keratin, porcine trypsin, bovine serum albumin, and their reversed sequences. Search parameters included enzyme specificity for trypsin allowing four missed cleavages with a tolerance of 20 ppm and 0.1 Da for MS and MS/MS mode, respectively. Variable modifications included cysteine carbamidomethylation, methionine oxidation, and serine, threonine, and tyrosine phosphorylation. All MS/MS spectra corresponding to reported phosphopeptides were identified with a score above the MASCOT homology threshold and were validated manually for diagnostic ions that identified the site of phosphorylation within the peptide.

ACKNOWLEDGMENTS

We thank the following for *C. elegans* strains: Bruce Bowerman, John White, Sander van den Heuvel, and the *Caenorhabditis* Genetics Center, which is funded by the National Institutes of Health Office of Research Infrastructure Programs (P40 OD010440). We thank Alex Mogilner for assistance in calculating frictional rotational drag. This work was supported by National Institute of General Medical Sciences Grant 1R01GM-079421 (to F.J.M.) and the University of California, Davis, Office of Research Campus Mass Spectrometry Facility (to A.A.).

REFERENCES

Albertson DG, Thomson JN (1993). Segregation of holocentric chromosomes at meiosis in the nematode, *Caenorhabditis elegans*. Chromosome Res 1, 15–26.

Bodenmiller B, Campbell D, Gerrits B, Lam H, Jovanovic M, Picotti P, Schlapbach R, Aebersold R (2008). PhosphoPep—a database of protein phosphorylation sites in model organisms. Nat Biotechnol 26, 1339–1340.

Colombo K, Grill SW, Kimple RJ, Willard FS, Siderovski DP, Gönczy P (2003). Translation of polarity cues into asymmetric spindle positioning in *Caenorhabditis elegans* embryos. Science 300, 1957–1961.

Connolly AA, Osterberg V, Christensen S, Price M, Lu C, Chicas-Cruz K, Lockery S, Mains PE, Bowerman B (2014). *Caenorhabditis elegans* oocyte meiotic spindle pole assembly requires microtubule severing and the calponin homology domain protein ASPM-1. Mol Biol Cell 25, 1298–1311.

Culver-Hanlon TL, Lex SA, Stephens AD, Quintyne NJ, King SJ (2006). A microtubule-binding domain in dynactin increases dynein processivity by skating along microtubules. Nat Cell Biol 8, 264–270.

Dorn JF, Zhang L, Paradis V, Edoh-Bedi D, Jusu S, Maddox PS, Maddox AS (2010). Actomyosin tube formation in polar body cytokinesis requires Anillin in *C. elegans*. Curr Biol 20, 2046–2051.

Ellefson ML, McNally FJ (2009). Kinesin-1 and cytoplasmic dynein act sequentially to move the meiotic spindle to the oocyte cortex in *Caenorhabditis elegans*. Mol Biol Cell 20, 2722–2730.

Ellefson ML, McNally FJ (2011). CDK-1 inhibits meiotic spindle shortening and dynein-dependent spindle rotation in *C. elegans*. J Cell Biol 193, 1229–1244.

Endow SA, Komma DJ (1997). Spindle dynamics during meiosis in *Drosophila* oocytes. J Cell Biol 137, 1321–1336.

Fabritius AS, Flynn JR, McNally FJ (2011). Initial diameter of the polar body contractile ring is minimized by the centralspindlin complex. Dev Biol 359, 137–148.

Flemming AJ, Shen ZZ, Cunha A, Emmons SW, Leroi AM (2000). Somatic polyploidization and cellular proliferation drive body size evolution in nematodes. Proc Natl Acad Sci USA 97, 5285–5290.

Goga A, Yang D, Tward AD, Morgan DO, Bishop JM (2007). Inhibition of CDK1 as a potential therapy for tumors over-expressing MYC. Nat Med 13, 820–827.

Gotta M, Dong Y, Peterson YK, Lanier SM, Ahringer J (2003). Asymmetrically distributed *C. elegans* homologs of AGS3/PINS control spindle position in the early embryo. Curr Biol 13, 1029–1037.

Kamath RS, Martinez-Campos M, Zipperlen P, Fraser AG, Ahringer J (2001). Effectiveness of specific RNA-mediated interference through ingested double-stranded RNA in *Caenorhabditis elegans*. Genome Biol 2, RESEARCH0002.

Kardon JR, Reck-Peterson SL, Vale RD (2009). Regulation of the processivity and intracellular localization of Saccharomyces cerevisiae dynein by dynactin. Proc Natl Acad Sci USA 106, 5669–5674.

Kincaid MM, King SJ (2006). Motors and their tethers: the role of secondary binding sites in processive motility. Cell Cycle 5, 2733–2737.

Kirby C, Kusch M, Kemphues K (1990). Mutations in the par genes of Caenorhabditis elegans affect cytoplasmic reorganization during the first cell cycle. Dev Biol 142, 203–215.

Kiyomitsu T, Cheeseman IM (2013). Cortical dynein and asymmetric membrane elongation coordinately position the spindle in anaphase. Cell 154, 391–402.

Kotak S, Gönczy P (2013). Mechanisms of spindle positioning: cortical force generators in the limelight. Curr Opin Cell Biol 25, 741–748.

Kozlowski C, Srayko M, Nedelec F (2007). Cortical microtubule contacts position the spindle in *C. elegans* embryos. Cell 129, 499–510.

Lu MS, Johnston CA (2013). Molecular pathways regulating mitotic spindle orientation in animal cells. Development 140, 1843–1856.

Lutz DA, Hamaguchi Y, Inoué S (1988). Micromanipulation studies of the asymmetric positioning of the maturation spindle in *Chaetopterus sp.* oocytes: I. Anchorage of the spindle to the cortex and migration of a displaced spindle. Cell Motil Cytoskeleton 11, 83–96.

Maro B, Johnson MH, Pickering SJ, Flach G (1984). Changes in actin distribution during fertilization of the mouse egg. J Embryol Exp Morphol 81, 211–237.

McCarter J, Bartlett B, Dang T, Schedl T (1999). On the control of oocyte meiotic maturation and ovulation in *Caenorhabditis elegans*. Dev Biol 205, 111–128.

McNally FJ (2013). Mechanisms of spindle positioning. J Cell Biol 200, 131–140.

McNally K, Audhya A, Oegema K, McNally FJ (2006). Katanin controls mitotic and meiotic spindle length. J Cell Biol 175, 881–891.

McNally KL, Martin JL, Ellefson M, McNally FJ (2010). Kinesin-dependent transport results in polarized migration of the nucleus in oocytes and inward movement of yolk granules in meiotic embryos. Dev Biol 339, 126–140.

McNally KP, Buster D, McNally FJ (2002). Katanin-mediated microtubule severing can be regulated by multiple mechanisms. Cell Motil Cytoskeleton 53, 337–349.

McNally KP, McNally FJ (2011). The spindle assembly function of *Caenorhabditis elegans* katanin does not require microtubule-severing activity. Mol Biol Cell 22, 1550–1560 [correction published in Mol Biol Cell (2012). 23, 4472].

Moore JK, Sept D, Cooper JA (2009). Neurodegeneration mutations in dynactin impair dynein-dependent nuclear migration. Proc Natl Acad Sci USA 106, 5147–5152.

Motegi F, Velarde NV, Piano F, Sugimoto A (2006). Two phases of astral microtubule activity during cytokinesis in *C. elegans* embryos. Dev Cell 10, 509–520.

Nguyen-Ngoc T, Afshar K, Gönczy P (2007). Coupling of cortical dynein and G alpha proteins mediates spindle positioning in *Caenorhabditis elegans*. Nat Cell Biol 9, 1294–1302.

Nicholas MP, Höök P, Brenner S, Wynne CL, Vallee RB, Gennerich A (2015). Control of cytoplasmic dynein force production and processivity by its C-terminal domain. Nat Commun 6, 6206.

Palazzo RE, Vogel JM (1999). Isolation of centrosomes from *Spisula solidissima* oocytes. Methods Cell Biol 61, 35–56.

Srayko M, Kaya A, Stamford J, Hyman AA (2005). Identification and characterization of factors required for microtubule growth and nucleation in the early *C. elegans* embryo. Dev Cell 9, 223–236.

Srinivasan DG, Fisk RM, Xu H, van den Heuvel S (2003). A complex of LIN-5 and GPR proteins regulates G protein signaling and spindle function in *C elegans*. Genes Dev 17, 1225–1239.

Timmons L, Court DL, Fire A (2001). Ingestion of bacterially expressed dsRNAs can produce specific and potent genetic interference in *Caenorhabditis elegans*. Gene 263, 103–112.

van der Voet M, Berends CW, Perreault A, Nguyen-Ngoc T, Gonczy P, Vidal M, Boxem M, van den Heuvel S (2009). NuMA-related LIN-5, ASPM-1, calmodulin and dynein promote meiotic spindle rotation independently of cortical LIN-5/GPR/Galpha. Nat Cell Biol 11, 269–277.

Villerbu N, Gaben AM, Redeuilh G, Mester J (2002). Cellular effects of purvalanol A: a specific inhibitor of cyclin-dependent kinase activities. Int J Cancer 97, 761–769.

Wachsstock DH, Schwartz WH, Pollard TD (1993). Affinity of alpha-actinin for actin determines the structure and mechanical properties of actin filament gels. Biophys J 65, 205–214.

Wang Q, Racowsky C, Deng M (2011). Mechanism of the chromosome-induced polar body extrusion in mouse eggs. Cell Div 6, 17.

Waterman-Storer CM, Karki S, Holzbaur EL (1995). The p150Glued component of the dynactin complex binds to both microtubules and the actin-related protein centractin (Arp-1). Proc Natl Acad Sci USA 92, 1634–1638.

Weisbrich A, Honnappa S, Jaussi R, Okhrimenko O, Frey D, Jelesarov I, Akhmanova A, Steinmetz MO (2007). Structure-function relationship of CAP-Gly domains. Nat Struct Mol Biol 14, 959–967.

Xu J, Wirtz D, Pollard TD (1998). Dynamic cross-linking by alpha-actinin determines the mechanical properties of actin filament networks. J Biol Chem 273, 9570–9576.

Yamada S, Wirtz D, Kuo SC (2000). Mechanics of living cells measured by laser tracking microrheology. Biophys J 78, 173–747.

Yang HY, Mains PE, McNally FJ (2005). Kinesin-1 mediates translocation of the meiotic spindle to the oocyte cortex through KCA-1, a novel cargo adapter. J Cell Biol 169, 447–457.

Yang HY, McNally K, McNally FJ (2003). MEI-1/katanin is required for translocation of the meiosis I spindle to the oocyte cortex in *C. elegans*. Dev Biol 260, 245–259.

Zielinska DF, Gnad F, Jedrusik-Bode M, Wiśniewski JR, Mann M (2009). *Caenorhabditis elegans* has a phosphoproteome atypical for metazoans that is enriched in developmental and sex determination proteins. J Proteome Res 8, 4039–4049.